Chemical Engineering Journal 158 (2010) 281–289

Contents lists available at ScienceDirect

Chemical Engineering Journal

journal homepage: www.elsevier.com/locate/cej

Numerical prediction of particle dispersions in downer under different gravity environments

Yang Liu [a,*], Guohui Li [b]

[a] Marine Engineering College, Dalian Maritime University, Linghai Road 1, Dalian 116026, Liaoning, China
[b] School of Electronic and Information Engineering, Dalian Jiaotong University, Dalian 116028, China

ARTICLE INFO

Article history:
Received 6 December 2009
Received in revised form 20 January 2010
Accepted 21 January 2010

Keywords:
Unified-second-order-moment model
Gravity
Downer
Dense gas–particle flows
Numerical simulation

ABSTRACT

Particle dispersion behavior of dense gas–particle flows in a downer affected by gravity environment is numerically simulated using an Euler–Euler two-fluid approach incorporating unified-second-order-moment two-phase turbulent models and kinetic theory of granular flows (USM-θ). Anisotropy of gas–solid two-phase stress and the interaction between two-phase stresses are fully considered by two-phase Reynolds stress model and the transport equation of two-phase stress correlation. The flow behavior of particles in a downer of Wang et al. (1992) [27] experiments is predicted under earth gravity, lunar gravity and microgravity environment. Simulation results of particle concentration and particle velocity are in good agreement with measurement data under earth gravity environment. Comparison earth gravity to lunar and microgravity condition, peak value of particle concentration is shifted to near center region and axial particle fluctuation velocity is larger than that of approximately 3.0 times. Particle temperature, particle heterogeneities dispersion and particle–particle collision are weakened due to decrease gravity. Furthermore, roles of particle and gas kinetic energy in particle–fluid system are alternated. Both particle kinetic energy and gas kinetic energy are greater than ones under earth gravity conditions.

1. Introduction

In order to acquire a rare mineral resource (i.e. helium III) for solving energy crisis of human being in lunar or deep space stellar, it is important for us to clearly understand the mechanism of particle–fluid system under different space gravity environment. Lunar gravitational acceleration is approximately equal to the one-sixth of earth and differs from other planets such as Mars, Mercury, etc., with the microgravity environment with 10^{-2} to 10^{-3} times by earth gravity [1–3]. Microgravity environment obtained by the ground-based test is very difficult to achieve. Therefore, numerical simulation validated by ground-based test predicting hydrodynamics of particle–fluid system under other gravity environment is necessary. Dense gas–particle flows are encountered in fluidized beds, riser and downer reactors and near wall zone of dilute swirling gas–particle flows. With many advantages such as good gas–solids contact, less gas and solids back-mixing, a short contact time and more uniform residence time distribution compared with the up-flow fast fluidized bed riser, downer reactors become more advantageous over risers for reactions of very short residence time and reactions where the intermediates are the desirable products [4–13].

Particle–particle collision plays an important role in behavior of two-phase turbulence flows. Computational fluid dynamics (CFD) with an Eulerian–Eulerian two-fluid modeling approaches have been widely used to predict hydrodynamics in circulated fluidized bed (CFB). In this scheme, the constitutive relation for particle–particle collision may be obtained from the kinetic theory of granular flow proposed by Lun et al. [14] and Gidaspow and co-worker [28]. Numerical studies have shown the capability of this kinetic theory approach for modeling downers. This theory is similar to an analogy between the dense gas kinetic theory and the particle random fluctuation due to particle collision, which causes the transfer of particle momentum and produces particle pressure and viscosity. Particle pressure and viscosity depend on the magnitude of small-scale particle fluctuations. It can be described by the particle pseudo-thermal energy from the particle stress and dissipating through the inelastic collisions between particles. Savage [15] and Gidaspow [16] derived the full equations of kinetic theory for granular flows. Sinclair and Jackson [17] first applied this theory to set up a laminar gas-phase and laminar particle-phase model to simulate the fully developed flow in vertical pipes. Considering the effect of gas turbulence, Bolio et al. [18] accounted for both gas turbulence modeled by a low Renumber k–ε model and particle fluctuation due to collision. Lu and Gidaspow [10], Lu et al. [19]

* Corresponding author. Tel.: +86 411 13889538128.
E-mail addresses: liuya@mail.tsinghua.edu.cn, yangliu@dlmu.edu.cn (Y. Liu).

1385-8947/$ – see front matter © 2010 Elsevier B.V. All rights reserved.
doi:10.1016/j.cej.2010.01.047

and Wang et al. [20] simulate the gas–particle flow in riser reactors using the kinetic theory, in which the gas turbulence is modeled using large eddy simulation. All of these studies considered that the particle flow is laminar flow and is not turbulence flow. Thus, large-scale fluctuation from particle turbulence is neglected. So, Zhou [21], Zhou et al. [22], Zhou and Chen [23] and Liu et al. [24] proposed a k–ε–k_p model, a USM and a sub-grid scale USM model to simulate gas–particle turbulence flows. USM model can fully consider both the anisotropy of gas–solid two-phase stresses and the interaction between two-phase stresses using two-phase Reynolds stress model using two-phase Reynolds stress incorporated with the transport equation of two-phase stress correlation correlations. Cheng et al. [6] proposed a k–ε–k_p–Θ dense gas–particle two-phase flow four equation model and Zheng et al. [25] established a k–ε–k_p–ε_p–Θ dense gas–particle two-phase flow five equation model to successfully simulate the downer and riser particle turbulence. Those simulated results well agreed with experimental data. It demonstrates that this idea of small-scale fluctuations due to particle–particle collision and large-scale fluctuations due to particle turbulence is reasonable.

To date, particle dispersion behavior in downer under earth gravity, microgravity and lunar gravity environment have never been reported. In the paper, USM-θ model is used to study and discuss for the mechanism of particle dispersion behavior affected by gravity environment.

2. Conservation equations for gas and particle flows

Conservation equations in two-fluid model for gas and particle flows with constitutive relations and closure model, is listed below.

2.1. Continuity and moment equations

The continuity equations for gas (k = gas) and particle (k = particle) are:

$$\frac{\partial}{\partial t}(\alpha_k\rho_k)+\frac{\partial}{\partial x_j}(\alpha_k\rho_k\overline{u_{ki}})=0 \tag{1}$$

where α_k is the volume fraction of phase k, u_{ki} the velocity vector of phase k, and ρ_k the density of phase k.

The momentum balance equation for the gas-phase and particle-phase are:

$$\frac{\partial(\alpha_g\rho_g\overline{u_{gi}})}{\partial t}+\frac{\partial(\alpha_g\rho_g\overline{u_{gk}u_{gi}})}{\partial x_k} = S_g-\alpha_g\frac{\partial\overline{p}}{\partial x_i}+\frac{\partial}{\partial x_k}(\tau_{gik}-\alpha_g\rho_g\overline{u'_{gi}u'_{gk}})-\beta(\overline{u_{gi}}-\overline{u_{si}}) \tag{2}$$

$$\frac{\partial(\alpha_p\rho_p\overline{u_{si}})}{\partial t}+\frac{\partial(\alpha_p\rho_p\overline{u_{pk}u_{pi}})}{\partial x_k} = S_p-\alpha_p\frac{\partial\overline{p}}{\partial x_i}-\frac{\partial\overline{p_p}}{\partial x_i}+\frac{\partial}{\partial x_k}(\tau_{pik}-\alpha_p\rho_p\overline{u'_{pk}u'_{pi}})+\beta(\overline{u_{gi}}-\overline{u_{pi}}) \tag{3}$$

where $S_g=\alpha_g\rho_g g$ and $S_p=\alpha_p\rho_p g$ is the gravity source term for gas- and particle-phase to consider the affected by gravity environment, g the gravity acceleration, p the thermodynamic pressure, β the interface momentum transfer coefficient, respectively. τ_g and τ_p are gas-phase and particle-phase viscous stress tensor, they are closed by:

$$\tau_{g,ij}=\mu_{gl}\left(\frac{\partial\overline{u_{gi}}}{\partial x_j}+\frac{\overline{\partial u_{gj}}}{\partial x_i}\right)-\frac{2}{3}\mu_{gl}\frac{\partial\overline{u_{gj}}}{\partial x_j}\delta_{ij} \tag{4}$$

$$\tau_{p,ij}=\mu_{p}\left(\frac{\partial\overline{u_{pi}}}{\partial x_j}+\frac{\partial\overline{u_{pj}}}{\partial x_i}\right)-\frac{2}{3}\mu_{p}\frac{\partial\overline{u_{pj}}}{\partial x_j}\delta_{ij} \tag{5}$$

2.2. Interphase moment exchange

In order to couple the momentum transfer between gas- and particle-phase, a model for the drag force is required. For porosities less than 0.8, the pressure drop due to friction between gas and particles can be described by the Ergun equation. For porosities greater than 0.8, Wen and Yu equation was used:

$$\beta=150\frac{\alpha_p^2\mu_g}{\alpha_g d_p^2}+1.75\frac{\alpha_p\rho_g\left|\vec{u}_g-\vec{u}_p\right|}{d_p},\quad \alpha_g<0.8 \tag{6}$$

$$\beta=\frac{3}{4}C_D\frac{\alpha_p\rho_g\left|\vec{u}_g-\vec{u}_p\right|}{d_p}\alpha_g^{-2.65},\quad \alpha_g\geq 0.8 \tag{7}$$

$$C_D=\frac{24}{Re_p}(1+0.15Re_p^{0.687}),\quad Re_p\leq 1000 \tag{8}$$

$$C_D=0.44,\quad Re_p>1000 \tag{9}$$

$$Re_p=\frac{\alpha_g\rho_g d_p\left|\vec{u}_g-\vec{u}_p\right|}{\mu_g} \tag{10}$$

2.3. Reynolds stress equations of gas- and particle-phase

The gas Reynolds stress equation is:

$$\frac{\partial(\alpha_g\rho_g\overline{u'_{gi}u'_{gj}})}{\partial t}+\frac{\partial(\alpha_g\rho_g\overline{u_{gk}}\cdot\overline{u'_{gi}u'_{gj}})}{\partial x_k} = D_{g,ij}+P_{g,ij}+\Pi_{g,ij}-\varepsilon_{g,ij}+G_{g,gp,ij} \tag{11}$$

where the terms on the right-hand side of Eq. (11) stand for the diffusion term, shear production term, pressure–strain term, dissipation term and gas–particle interaction term, respectively. They are closed as follows:

$$D_{g,ij}=\frac{\partial}{\partial x_k}\left(C_g\alpha_g\rho_g\frac{k_g}{\varepsilon_g}\overline{u'_{gk}u'_{gl}}\frac{\partial\overline{u'_{gi}u'_{gj}}}{\partial x_l}\right) \tag{12}$$

$$P_{g,ij}=-\alpha_g\rho_g\left(\overline{u'_{gk}u'_{gj}}\frac{\partial\overline{u_{gi}}}{\partial x_k}+\overline{u'_{gk}u'_{gi}}\frac{\partial\overline{u_{gj}}}{\partial x_k}\right) \tag{13}$$

$$\prod_{g,ij}=\prod_{g,ij,1}+\prod_{g,ij,2}=-C_{g1}\frac{\varepsilon_g}{k_g}\alpha_g\rho_g\left(\overline{u'_{gi}u'_{gj}}-\frac{2}{3}k_g\delta_{ij}\right)-C_{g2}\left(P_{g,ij}-\frac{2}{3}P_g\delta_{ij}\right) \tag{14}$$

$$P_g=-\alpha_g\rho_g\overline{u'_{gk}u'_{gi}}\frac{\partial\overline{u_{gi}}}{\partial x_k} \tag{15}$$

$$G_{g,gp,ij}=\beta(\overline{u'_{pi}u'_{gj}}+\overline{u'_{gi}u'_{pj}}-2\overline{u'_{gi}u'_{gj}}) \tag{16}$$

The particle Reynolds stress equation is:

$$\frac{\partial(\alpha_p\rho_p\overline{u'_{pi}u'_{pj}})}{\partial t}+\frac{\partial(\alpha_p\rho_p\overline{u_{pk}}\cdot\overline{u'_{pi}u'_{pj}})}{\partial x_k} = D_{p,ij}+P_{p,ij}+\Pi_{p,ij}-\varepsilon_{p,ij}+G_{p,gp,ij} \tag{17}$$

where the terms on the right-hand side of Eq. (17) stand for the diffusion term, shear production term, pressure–strain term, dissipation term and gas–particle interaction term, respectively. They are closed as follows:

$$D_{p,ij}=\frac{\partial}{\partial x_k}\left(C_s\alpha_p\rho_p\frac{k_p}{\varepsilon_p}\overline{u'_{pk}u'_{pl}}\frac{\partial\overline{u'_{pi}u'_{pj}}}{\partial x_l}\right) \tag{18}$$

$$P_{p,ij}=-\alpha_p\rho_p\left(\overline{u'_{pk}u'_{pj}}\frac{\partial\overline{u_{pi}}}{\partial x_k}+\overline{u'_{pk}u'_{pi}}\frac{\partial\overline{u_{pj}}}{\partial x_k}\right) \tag{19}$$

$$\prod_{p,ij} = \prod_{p,ij,1} + \prod_{p,ij,2} = -C_{p1}\frac{\varepsilon_p}{k_p}\alpha_p\rho_p\left(\overline{u'_{pi}u'_{pj}} - \frac{2}{3}k_p\delta_{ij}\right) - C_{p2}\left(P_{p,ij} - \frac{2}{3}P_p\delta_{ij}\right) \quad (20)$$

$$\varepsilon_{p,ij} = \frac{2}{3}\delta_{ij}\alpha_p\rho_p\varepsilon_p \quad (21)$$

$$G_{p,gp,ij} = \beta(\overline{u'_{pi}u'_{gj}} + \overline{u'_{pj}u'_{gi}} - 2\overline{u'_{pi}u'_{pj}}) \quad (22)$$

For dense gas–particle flows, pressure–strain term and dissipation term caused by particle pressure P_p and particle viscosity shear stress $\varepsilon_{p,ij}$ for particle–particle collision. It results in the redistribution and dissipation of particle Reynolds stress in every direction. Thus, particle temperature is incorporated into USM model.

2.4. Dissipation transport equations of turbulent kinetic energy

Dissipation transport equations of turbulent kinetic energy for gas- and particle-phase are:

$$\frac{\partial(\alpha_g\rho_g\varepsilon_g)}{\partial t} + \frac{\partial(\alpha_g\rho_g\overline{u_{gk}}\varepsilon_g)}{\partial x_k} = \frac{\partial}{\partial x_k}\left(C_g\alpha_g\rho_g\frac{k_g}{\varepsilon_g}\overline{u'_{gk}u'_{gl}}\frac{\partial\varepsilon_g}{\partial x_l}\right) + \frac{\varepsilon_g}{k_g}\left[c_{\varepsilon1}(P_g + G_{g,gp}) - c_{\varepsilon2}\alpha_g\rho_g\varepsilon_g\right] \quad (23)$$

$$\frac{\partial(\alpha_p\rho_p\varepsilon_p)}{\partial t} + \frac{\partial(\alpha_p\rho_p\overline{u_{pk}}\varepsilon_p)}{\partial x_k} = \frac{\partial}{\partial x_k}\left(\alpha_p\rho_pC_p^d\frac{k_p}{\varepsilon_p}\overline{u'_{pk}u'_{pl}}\frac{\partial\varepsilon_p}{\partial x_l}\right) + \frac{\varepsilon_p}{k_p}\left[C_{\varepsilon p,1}(P_p + G_{p,gp}) - C_{\varepsilon p,2}\alpha_p\rho_p\varepsilon_p\right] \quad (24)$$

where

$$P_g = -\alpha_g\rho_g\overline{u'_{gk}u'_{gi}}\frac{\partial\overline{u_{gi}}}{\partial x_k} \quad (25)$$

$$P_p = -\varepsilon_p\rho_p\overline{u'_{pi}u'_{pk}}\frac{\partial\overline{u_{pi}}}{\partial x_k} \quad (26)$$

As for the interaction correlation term of gas–particle turbulence, Zhou and Chen [23] established the simply closed correlations using a non-dimensional analysis, and kinetic energy is always greater than zero. But, it is found that it always smaller than gas and particle kinetic energy in many experiments. That is it means the negative existing. Therefore, it is reasonable that this term will be dealt with a turbulence dissipation term for gas–particle-phase. Mohanarangam and Tu [26] proposed the correlation transportation equation based on the isotropic turbulence kinetic energy (scalar quantity). Only the shortcoming is that the closed transportation equation cannot reflect the anisotropic turbulence flows. In this works, interaction correlation term indicating anisotropic gas–particle two-phase turbulence flows can be modeled by the following transport equation:

$$\frac{\partial\overline{u'_{pi}u'_{gj}}}{\partial t} + (\overline{u_{gk}} + \overline{u_{pk}})\frac{\partial\overline{u'_{pi}u'_{gj}}}{\partial x_k} = D_{gp,ij} + P_{gp,ij} + \Pi_{gp,ij} - \varepsilon_{gp,ij} + T_{gp,ij} \quad (27)$$

where the terms on the right-hand-side stand for the diffusion term, shear production term, pressure–strain term, dissipation term and gas–particle interaction term, respectively. They are closed as follows:

$$D_{gp,ij} = \frac{\partial}{\partial x_k}\left(C_{gp,3}\left(\frac{k_p}{\varepsilon_p}\overline{u'_{pk}u'_{pl}} + \frac{k_g}{\varepsilon_g}\overline{u'_{gk}u'_{gl}}\right)\frac{\partial\overline{u'_{gi}u'_{pj}}}{\partial x_l}\right) \quad (28)$$

$$P_{gp,ij} = -\overline{u'_{pi}u'_{gk}}\frac{\partial\overline{u_{gj}}}{\partial x_k} - \overline{u'_{pk}u'_{gj}}\frac{\partial\overline{u_{pi}}}{\partial x_k} \quad (29)$$

$$P_{gp} = -\frac{1}{2}\left(\overline{u'_{pi}u'_{gk}}\frac{\partial\overline{u_{gi}}}{\partial x_k} + \overline{u'_{pk}u'_{gi}}\frac{\partial\overline{u_{pi}}}{\partial x_k}\right) \quad (30)$$

$$\prod_{gp,ij} = \prod_{gp,ij,1} + \prod_{gp,ij,2} = -\frac{C_{gp,1}}{\tau_{rp}}\left(\overline{u'_{pi}u'_{gj}} - \frac{2}{3}k_{gp}\delta_{ij}\right) - C_{gp,2}\left(P_{gp,ij} - \frac{2}{3}P_{gp}\delta_{ij}\right) \quad (31)$$

$$T_{gp,ij} = \frac{\beta}{\alpha_g\rho_g\alpha_p\rho_p}(\alpha_p\rho_p\overline{u'_{pi}u'_{pj}} + \alpha_g\rho_g\overline{u'_{gi}u'_{gj}} - (\alpha_g\rho_g + \alpha_p\rho_p)\overline{u'_{gj}u'_{pi}}) \quad (32)$$

$$\varepsilon_{gp,ij} = \frac{\overline{u'_{pi}u'_{gj}}}{\min(\tau_{rp}, (k_p/\varepsilon_p))} \quad (33)$$

2.5. Equations of particle temperature

The conservation equation of particle fluctuating energy or translational granular temperature is:

$$\frac{3}{2}\left[\frac{\partial(\alpha_p\rho_p\theta)}{\partial t} + \frac{\partial(\alpha_p\rho_p\overline{u_{pk}}\theta)}{\partial x_k}\right] = \frac{\partial}{\partial x_k}\left(C_p\alpha_p\rho_p\frac{k_p^2}{\varepsilon_p}\right) + \frac{\partial}{\partial x_k}\left(k_p\frac{\partial\theta}{\partial x_k}\right) + \mu_p\left(\frac{\partial\overline{u_{pk}}}{\partial x_i} + \frac{\partial\overline{u_{pi}}}{\partial x_k}\right)\frac{\partial\overline{u_{pi}}}{\partial x_k} + \mu_p\varepsilon_p - \overline{p_p}\frac{\partial\overline{u_{pl}}}{\partial x_l} + \left(\xi_p - \frac{2}{3}\mu_p\right)\left(\frac{\partial\overline{u_{pl}}}{\partial x_l}\right)^2 - \gamma_p \quad (34)$$

where k_p is the conductivity coefficient of granular temperature, it is as follows:

$$k_p = \frac{150}{384(1+e)g_0}\rho_pd_p\sqrt{\pi\theta}\left[1 + \frac{6}{5}(1+e)g_0\alpha_p\right]^2 + 2\alpha_p^2\rho_pd_pg_0(1+e)\sqrt{\frac{\theta}{\pi}} \quad (35)$$

The translational fluctuation energy dissipation rate is:

$$\gamma_p = 3(1-e^2)\alpha_p^2\rho_pg_0\theta\left[\frac{4}{d_p}\sqrt{\frac{\theta}{\pi}} - \frac{\partial u_{pk}}{\partial x_k}\right] \quad (36)$$

The bulk solids viscosity is:

$$\xi_p = \frac{4}{3}\alpha_p^2\rho_pd_pg_0(1+e)\sqrt{\frac{\theta}{\pi}} \quad (37)$$

The radial distribution function g_0, can be seen as a measure for the probability of inter-particle correlation:

$$g_0 = \left[1 - \left(\frac{\alpha_p}{\alpha_{p,\max}}\right)^{1/3}\right]^{-1} \quad (38)$$

where d_p is the particle diameter, e the coefficient of particle restitution, $\varepsilon_{p,\max}$ is the particle maximum volume fraction at random packing.

The particle pressure represents the particle normal forces due to particle–particle interaction. It is calculated as follows:

$$P_p = \alpha_p\rho_p[1 + 2(1+e)\alpha_pg_0]\theta \quad (39)$$

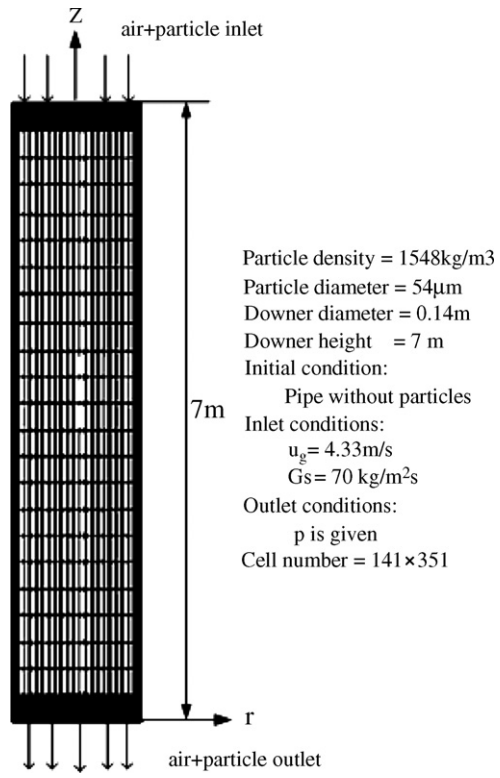

Fig. 1. Scheme drawing of 2D downer with inlet and initial conditions.

The equation of particle viscosity can be expressed as a function of granular temperature of the following equations:

$$\mu_p = \frac{2\mu_{p,\mathrm{dil}}}{(1+e)g_0}\left[1+\frac{4}{5}(1+e)g_0\alpha_p\right]^2 + \frac{4}{5}\alpha_p^2\rho_p d_p g_0(1+e)\sqrt{\frac{\theta}{\pi}} \quad (40)$$

$$\mu_{p,\mathrm{dil}} = \frac{5}{96}\rho_p d_p\sqrt{\pi\theta} \quad (41)$$

2.6. Boundary conditions and experiments

For boundary conditions, at the inlet, particle with a flat uniform velocity profile and air with a parabolic velocity profile are set. All velocity and volume fraction of both phase were specified. Averaged inlet superficial gas-phase velocity is 4.33 m/s. Particle volume fraction is 0.02. The normal components of Reynolds stresses are assumed to have an isotropic inlet distribution and the shear stresses are determined by eddy viscosity expressions. The turbulent kinetic energy and its dissipation rate are taken by empirical expressions. At the outlet, the fully developed flow conditions of two-phase are taken. At the wall, no slip condition is used for gas-phase velocity and gas Reynolds stress are determined via production term including the effect of wall function for near wall grid nodes. $(\partial\varphi/\partial x) = 0(\varphi = u_{g,p}, v_{g,p}, u'_{g,p}, \ldots)$. Particle-phase used a partial slip condition considering the wall roughness [8]. At the near wall grid nodes, the wall-function approximation is used. At the axis, symmetric conditions are adopted for both the two phase. The convergence criteria for gas- and particle-phase are mass source 1.0×10^{-4}. The code is written in Fortran-90 languages, consisting of 14000 statements. Empiric constants are showed in Table 1.

Table 1
Empiric constants.

c_1	c_2	c_μ	$c_{\varepsilon 1}$	$c_{\varepsilon 2}$	$c_{\mu p}$	c_{pg1}	c_{pg2}	$c_{\varepsilon p1}$	$c_{\varepsilon p2}$
1.8	0.6	0.09	1.44	1.92	0.09	1.8	0.6	2.5	1.5

Experiment for downer carried out by Wang et al. [27] is used to validate the simulation code under earth gravity environment. The downer is 7 m high with as diameter of 0.14 m. The average gas inlet velocity is 4.33 m/s and particles flow rates is $Gs = 70$ kg/(m^2 s). The particle-phase is fluidized catalytic cracking (FCC) particles with a size of 54 μm and material density is 1545 kg/m^3. The computa-

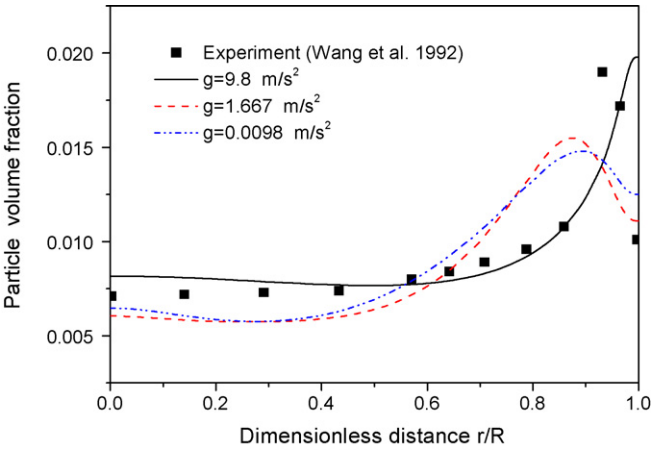

Fig. 3. Comparison of particle concentration.

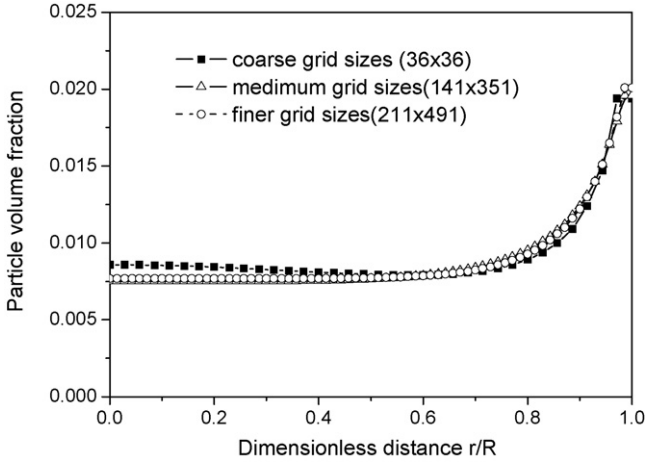

Fig. 2. Effects of grid sizes on particle concentration.

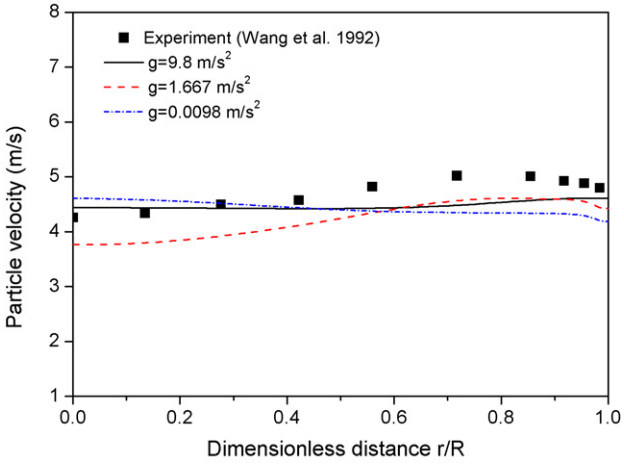

Fig. 4. Comparison of particle axial averaged velocity.

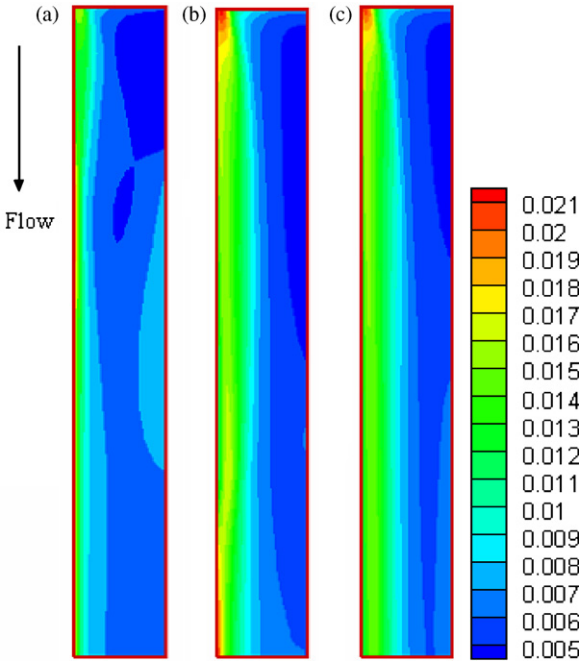

Fig. 5. Contour of particle concentration under different gravity environment (a, $g = 9.8\ m/s^2$; b, $g = 1.667\ m/s^2$; c, $g = 0.0098\ m/s^2$).

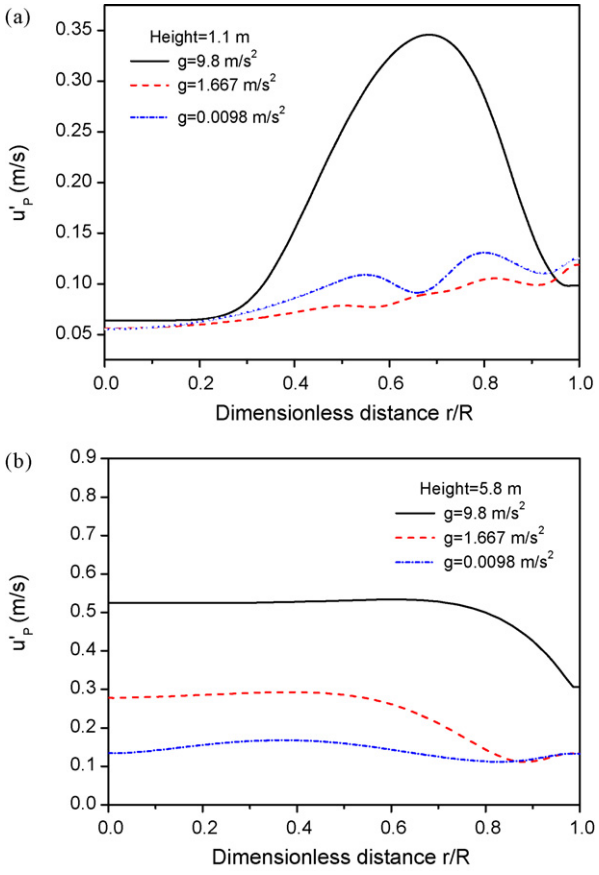

Fig. 6. Distribution of axial particle fluctuation velocity.

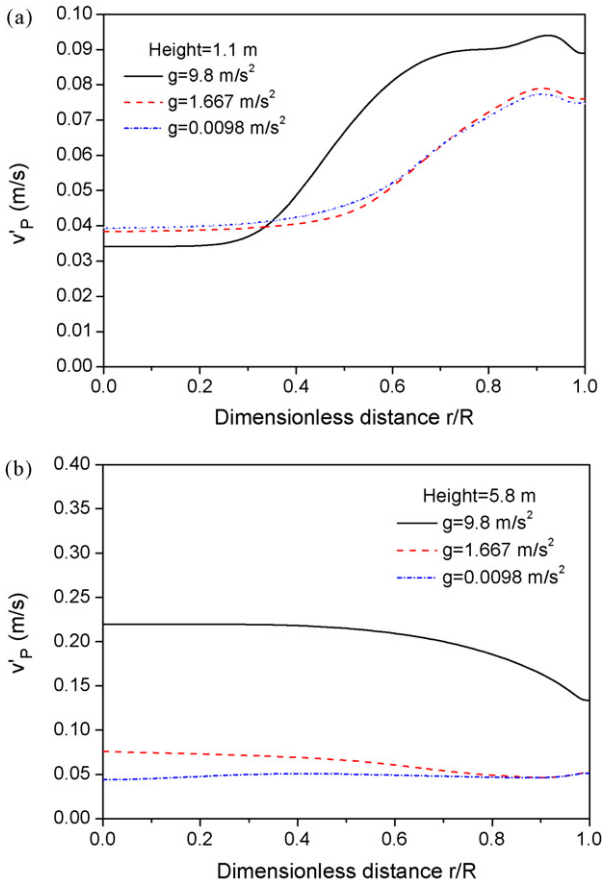

Fig. 7. Distribution of radial particle fluctuation velocity.

tional grid nodes are 141×351. The governing equations are solved by a finite volume method. The calculation domain is divided into a finite number of the control volumes. At main grid points placed in the center of the control volume, scalar quantity parameters such as the volume fraction of particles, density and turbulent kinetic energy are stored. A staggered grid arrangement is used and the velocity components are solved at the volume surfaces. The conservation equations are integrated in the space time and space. The finite differential equations are solved by semi-implicit pressure linked equations-corrected (SIMPLEC) algorithm to correct p–v correlation with tri-diagonal marching algorithm (TDMA) line-by-line iteration and under-relaxation.

3. Simulated results and discussions

In the experiment, hydrodynamics of co-current down-flow gas–solid suspension in circulating fluidized bed (CDCFB) reactor was measured. The parameters of the geometry, particle properties and computational mesh layout of CFB downer are shown in Fig. 1. Initially the downer column was empty and the velocities of both phases were assumed to be zero.

Sensitivity of computed particle concentration distribution to spatial grid sizes is tested. The qualitative impact of the grid on the distribution of particle concentration is shown in Fig. 2. Although the distribution of concentration exhibit the same trends along radial direction, the difference is obvious. The most significant discrepancy is located in the center region. An agreement results between medium and finer grid size is found. Therefore, the medium grid size is used to reduce the computation times.

Fig. 3 shows comparison of particle concentration under the earth, lunar and microgravity gravity environment ($g = 9.8\ m/s^2$ for

earth, $g = 1.667\ m/s^2$ for lunar and $g = 0.0098\ m/s^2$ for microgravity), respectively. Predicted results under earth gravity are agreed well with the experiment. The higher particle concentration phenomena located in near wall region with a peak value. Co-current two-phase flows with lower particle concentration as well as flat profile are in accordance with measured results. For lunar and microgravity conditions, peak value is shifted to near center region. Both peak value and central region value are less than those of earth gravity. Peak value will affect greatly the heat transfer, reaction time, abrasion, etc. The lower particle concentration formed at the wall zone, in which differs from that of earth. Furthermore, the distributions profile and value have a similarity characters.

These special phenomena for lunar and microgravity can be explained as follows: peak value indicates the maximum particle concentration is produced. As for higher particle concentration, effects of particle–particle collisions are obvious. It leads to take a greater influence on gas–particle behavior by means of energy dissipation and energy transportation. In fact, for the co-existence of single particle and clusters (higher particle concentration), energy will transfer to particles and drive them break from clusters and move independently. Therefore, peak value will take a greater influence on gas–particle behaviors. Although particles are going to cluster to some extents in downer, cluster system is loose relatively due to gravity effects. For $g = 9.8\ m/s^2$, the highest particle concentration is obtained near wall region. However, with decrease of gravity value, gravity effects are reduced. Effects of particle–particle collision and particle–wall collision are in dominance. "Compacted cluster", compared with "loose cluster" due to gravity effects, prevent particles from escaping. Under lunar and microgravity conditions, the maximum particle concentration deviated from near wall zone and the lower particle concentration is found at the wall zone. It is different entirely from that of earth gravity due to gravity effects.

As for the particle axial averaged velocity, simulated results under earth gravity are in good agreement with measured data (see Fig. 4). But there is still a little discrepancy with experiments. The reason is that particle rotation and particle friction stress was neglected in particle temperature model. This drawback is further to be improved in the future research. For other gravity, their values are almost unchanged. Especially, values in lunar gravity are less than others near central region. It means that the residence time of flows has a constants value basically. Therefore, presented mathematical model and calculating code are validated by experimental data under gravity conditions. It may be used to predict gas–particle hydrodynamics in downer under lunar and microgravity conditions, especially the ground-test validation should be further studied.

Fig. 5 gives the simulated contour of particle concentration under different gravity environment. Particle concentrations are higher near wall zone and are lower in center region. Under different gravity conditions, the coherent structure differed from core-annular structure in a riser can be found. At the same time, all the distribution tendency of particle concentration is similar. It indicates the flow structure has character of uniformity. However, it decreases gradually to center region.

Fig. 6a and b shows the simulated distribution of axial particle fluctuation velocity at the height section of 1.1 and 5.8 m, respectively. At the inlet, peak value can be found in Fig. 6a. under earth gravity and not found under other gravity. It can be seen that the fluctuation velocity is lower in the center and is higher near wall region. With the development of flow, fluctuation intensity is strengthened as well as fluctuation velocity is higher in the center and lower near wall region. When r/R is less than 0.7, fluctuation intensity profile is flat. Near wall region, fluctuation intensity profile is decreased. Under lunar gravity, fluctuation intensity is

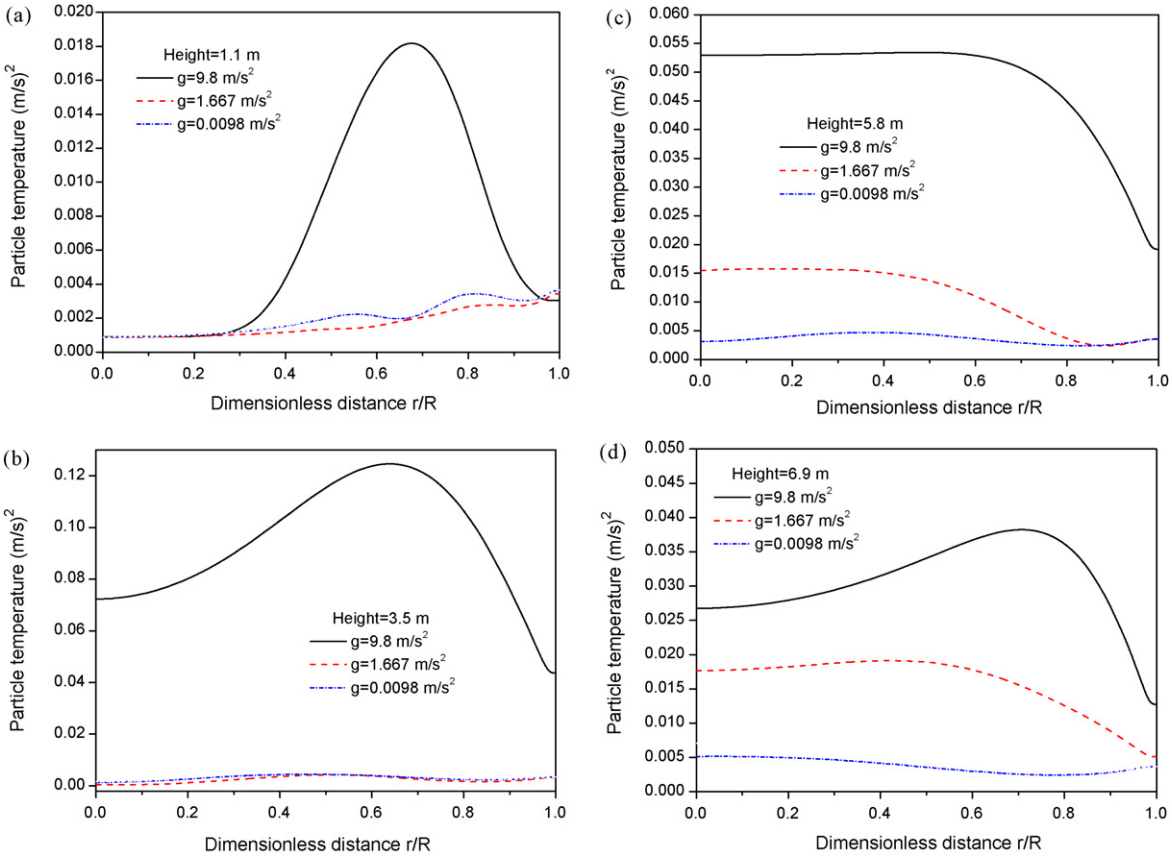

Fig. 8. Distribution of particle temperature.

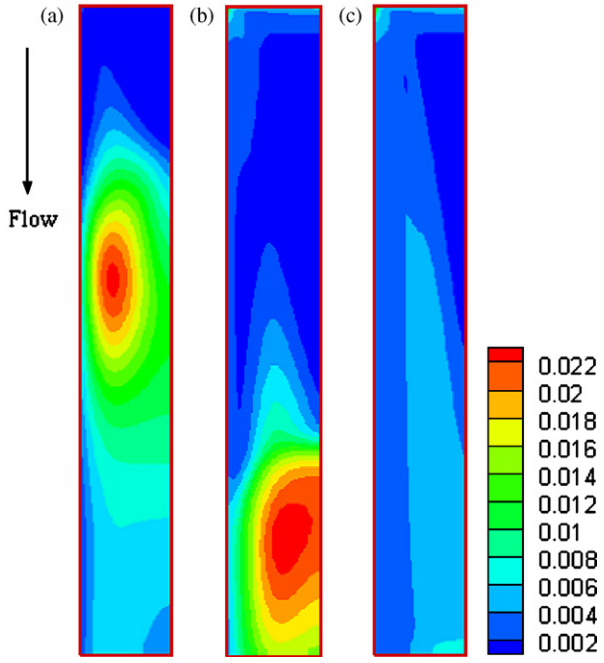

Fig. 9. Distribution of particle temperature with different gravity environment (a, $g = 9.8\ m/s^2$; b, $g = 1.667\ m/s^2$; c, $g = 0.0098\ m/s^2$).

less than that of earth gravity and larger than that of microgravity. Therefore, decrease of gravity leads to reduce the fluctuation intensity.

Fig. 7a and b shows the simulated distribution of radial particle fluctuation velocity at the height section of 1.1 and 5.8 m, respectively. Decrease of gravity value reduced greatly radial particle velocity fluctuation. But, it is enhanced the fluctuation at $r/R = 0.0–0.3$ and height = 1.1 m position. Radial fluctuation near wall region is larger than that of in center region at inlet, and is smaller at the fully development region. For lunar and microgravity, fluctuation keep a same level basically. Comparison of axial particle velocity fluctuation under earth gravity, it is approximately 3.0 times greater than that of lunar gravity and microgravity. The lower gravity, particle turbulence is lower. Thus, particle turbulence is affected by the particle–particle collision. Compared Fig. 7a to Fig. 7b, fluctuation in fully development region is larger than inlet region ones.

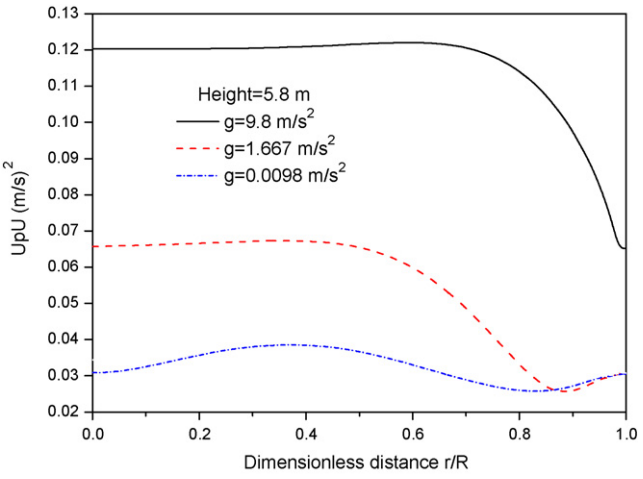

Fig. 10. Distribution of axial–axial fluctuation velocity correlation of gas and particle.

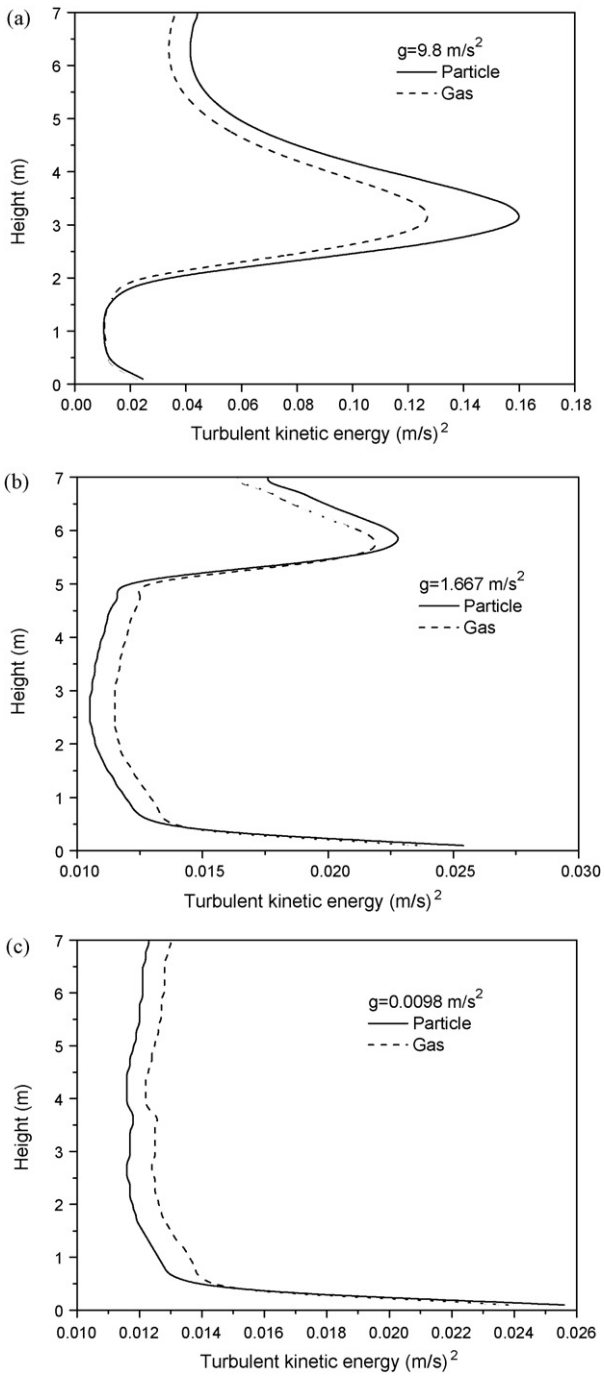

Fig. 11. Comparison of turbulent kinetic energy of gas- and particle-phase under different gravity environment.

Fig. 8a–d shows the simulated distribution of particle temperature at the height section of 1.1, 3.5, 5.8 and 6.9 m, respectively. It can be seen that particle temperature is lower near wall region and is higher in center region due to higher particle concentration with the greater energy decapitations. Under microgravity conditions, particle temperature near wall zone is slightly less than that of center region. This phenomena is thoroughly differ form that of earth condition. It indicates that effects of decreasing gravity value reduce greatly particle collision at center region with lower particle concentration. Decrease of gravity value, particle fluctuation is reduced due to particle–particle collisions. Under lower gravity conditions, particle temperature is lower and particle–particle collision is weaker. Decrease of gravity leads to reduce fluctua-

tion intensity. The lower gravity, particle temperature is lower and particle–particle collision is weaker. Compared Figs. 7 and 8, it can be seen that particle temperature due to particle–particle collisions is smaller than particle fluctuation both axial direction and radial direction.

Fig. 9a–d shows distribution of particle temperature with different gravity environment. Maximum particle temperature value is located in near wall region (see Fig. 9a) and is in near center region (see Fig. 9b). No obviously maximum value is found in Fig. 9c and d. Particle dispersion in the whole field is disturbed by gravity, and particle temperature reduced with the decrease of gravity value.

Fig. 10 shows distribution of axial–axial fluctuation velocity correlation of gas and particle. The gas–particle fluctuation velocity correlation is an important term in the USM two-phase turbulence model, which represents the turbulence interaction between the gas and particle Reynolds stresses. Decrease of gravity value reduced particle heterogeneities dispersion behavior in axial direction and had a little influence in radial direction. Comparison of Fig. 6b, it can be seen that axial particle velocity fluctuation $u_p u_p$ is about 4.5 times greater than that of $u_p u$. It indicates that particle dispersion presents the obvious anisotropic characters. Furthermore, gas and particle take on the different transport behavior for inertia action, in which is affected by gravity conditions.

Fig. 11 shows comparison of turbulent kinetic energy of gas- and particle-phase along downer height under different gravity environment. As we can see that particle kinetic energy is almost larger than gas and peak value is found at about the middle of downer (see Fig. 11a). As shown in Fig. 11b, particle kinetic energy is larger than that of gas at the outlet region. However, it is smaller than particle one at the middle and inlet region. From Fig. 11c and d, particle kinetic energy is smaller than that of gas at all the whole field section. Thus, the roles of particle and gas kinetic energy in particle–fluid system are alternated due to the decrease of gravity. Under earth gravity conditions, both particle and gas kinetic energy are grater greatly than those of other gravity conditions.

4. Conclusions

(1) The presented Euler–Euler two-fluid model with USM-θ for dense gas–particle flows in a downer considered fully the anisotropy of gas–solid two-phase stresses and the interaction between two-phase stresses are fully considered by two-phase Reynolds stress model and the transport equation of two-phase stress correlation.
(2) Under all of the earth, lunar and microgravity conditions, the gas–particle flow is uniform with flat velocity profile in center region.
(3) Decrease of gravity causes to reducing the particle fluctuation intensity, particle temperature and heterogeneities dispersion. Furthermore, particle concentration peaks is shifted to near center region.
(4) The roles of particle and gas kinetic energy in particle–fluid system are alternated due to the decrease of gravity. Under earth gravity conditions, both particle and gas kinetic energy are grater greatly than those of other gravity conditions.

Nomenclature

D	diffusion term
G	source term
k	kinetic energy
p	pressure
P	production term
R	correlation term
t	time
V, v	velocity

Greek alphabets

α	volume fraction
δ	Kronic–Delta unit tensor
ε	dissipation term
μ	dynamic viscosity
ν	kinematic viscosity
Π	pressure–strain term
ρ	density
τ	stress

Subscripts

i,j,k,l	coordinates directions
g,p	gas and particle
l	laminar
r	relaxation

Acknowledgments

We sincerely appreciate the financial support of Project No. 9078209 from China Academy of Space Technology and the Projects of National Natural Science Foundation of China under the Grants 50606026.

References

[1] P. Eckart, The Lunar Base Handbook—An Introduction to Lunar Base Design, Development and Operations, McGraw-Hill Companies, Inc., New York, 1999, pp. 851–864.
[2] K.B. David, R.L. Scott, Simulating lunar habitats and activities to derive system requirements, in: Proc. 1st Space Exploration Conference: Continuing the Voyage of Discovery, AIAA, 2005, pp. 2708–2720.
[3] K.M. Noreen, The lunar environment: determining the health effects of exposure to moon dusts, Acta Astronautica 63 (2008) 1006–1014.
[4] A. Srivastava, K. Agrawal, S. Sundaresan, S.B. Reddy, Dynamics of gas–particle flow in circulating fluidized beds, Powder Technology 100 (1998) 173–182.
[5] P. Lehner, K.E. Wirth, Characterization of the flow pattern in a downer reactor, Chemical Engineering Science 54 (1999) 5471–5483.
[6] Y. Cheng, Y.C. Guo, F. Wei, Modeling the hydrodynamics of downer reactors based on kinetic theory, Chemical Engineering Science 54 (1999) 2019–2027.
[7] W. Liu, K.B. Luo, J.X. Zhu, J.M. Beeckmans, Characterization of high-density gas–solids downward fluidized flow, Powder Technology 115 (2001) 27–35.
[8] M.H. Zhang, Q. Zhen, F. Wei, The near wall dense ring in a large-scale down-flow circulating fluidized bed, Chemical Engineering Journal 92 (2003) 161–167.
[9] S.G. Li, W.G. Lin, J.Z. Yao, Modeling of the hydrodynamics of the fully developed region in a downer reactor, Powder Technology 145 (2004) 73–81.
[10] H.L. Lu, D. Gidaspow, Hydrodynamics of binary fluidization in a riser: CFD simulation using two granular temperatures, Chemical Engineering Science 58 (2003) 3777–3792.
[11] X.S. Lu, S.G. Li, H.Z. Li, Flow structures in the downer circulating fluidized bed, Chemical Engineering Journal 112 (2005) 23–31.
[12] B.L. Luo, D. Yan, J. Zhu, Characteristics of gas–solid mass transfer in a co-current down-flow circulating fluidized bed reactor, Chemical Engineering Journal 132 (2007) 9–15.
[13] C.N. Wu, Y. Cheng, Y. Jin, Modeling the hydrodynamics in a coupled high density downer-to-riser reactor, Powder Technology 181 (2008) 255–265.
[14] C.K. Lun, S.B. Savage, D.J. Jeffrey, Kinetic theories for granular flow: inelastic particles in coquette flow and slightly inelastic particles in a general flow field, Journal of Fluid Mechanics 140 (1984) 223–256.
[15] S.B. Savage, Analysis of slow high-concentration flows of granular materials, Journal of Fluid Mechanics 377 (1998) 1–26.
[16] D. Gidaspow, Multiphase Flow and Fluidization: Continuum and Kinetic Theory Description, Academic Press, New York, 1994, pp. 65–78.
[17] J.L. Sinclair, R. Jackson, Gas–particle flow in a vertical pipe with particle–particle interaction, AIChE Journal 35 (1989) 1473–1486.
[18] E.J. Bolio, J.A. Yasuna, J.L. Sinclair, Dilute turbulent gas–solid flow in riser with particle–particle interactions, AIChE Journal 41 (1995) 1375–1388.
[19] H.L. Lu, W.T. Liu, R.S. Bie, D. Gidaspow, Kinetic theory of fluidized binary granular mixtures with unequal granular temperature, Physica A 284 (2000) 265–276.
[20] S.Y. Wang, Z.H. Shen, H.L. Lu, Numerical predictions of flow behavior and cluster size of particles in riser with particle rotation model and cluster-based approach, Chemical Engineering Science 63 (2008) 4116–4125.

[21] L.X. Zhou, Theory and Numerical Simulation Modeling of Turbulent Gas–Particle Flows and Combustion, Science Press/CRC Press, Beijing/Florida, 1993, pp. 13–21.
[22] L.X. Zhou, C.M. Liao, T. Chen, A unified second-order-moment two-phase turbulence model for simulating gas–particle flows, ASME Journal 185 (1994) 307–313.
[23] L.X. Zhou, T. Chen, Simulation of strongly swirling gas–particle flows using USM and k–ε–k_p two-phase turbulence models, Powder Technology 114 (2001) 1–11.
[24] Y. Liu, L.X. Zhou, C.X. Xu, Large-eddy simulation of swirling gas–particle flows using a USM two-phase SGS stress model, Powder Technology 198 (2009) 183–188.
[25] Y. Zheng, X.T. Wan, F. Wei, Y. Jin, Numerical simulation of the gas–particle turbulent flow in riser reactor based on k–ε–kp–εp–Θ two-fluid model, Chemical Engineering Science 56 (2001) 6813–6822.
[26] K. Mohanarangam, J.Y. Tu, Two-fluid model for particle-turbulence interaction in a backward-facing step, AICHE. Journal 53 (2007) 2254–2264.
[27] Y. Wang, D.R. Bai, Y. Jin, Hydrodynamics of concurrent downflow circulating fluidized bed (CDCFB), Powder Technology 70 (1992) 271–275.
[28] J. Ding, D. Gidaspow, A bubbling fluidization model with kinetic theory of granular flow, AIChE Journal 36 (1990) 523–538.